ADVANCED OPTICAL MATERIALS
www.advopticalmat.de

Diarylethenes in Optically Switchable Organic Light-Emitting Diodes: Direct Investigation of the Reversible Charge Carrier Trapping Process

Giovanni F. Cotella, Aurelio Bonasera, Giuseppe Carnicella, Alessandro Minotto, Stefan Hecht,* and Franco Cacialli**

The design, fabrication, and characterization of optically switchable organic light-emitting diodes (OSOLEDs) based on the combination of the commercially available light-emitting polymer poly(9,9′-dioctylfluorene-*alt*-benzothiadiazole), F8BT, doped with a diarylethene derivative is reported. The photochromic activity of the dopant in the solid state has been investigated both via UV/vis absorption and photoluminescence spectroscopy, whereas the morphology of different blends is investigated via atomic force microscopy. OSOLEDs embedding dopant loadings of 1, 5, and 10 wt% exhibit optical responsivity with a maximum reversible optical threshold voltage shift of 4 V. The best performing devices containing 5 wt% dopant show a maximum current density and luminance ON/OFF ratio of ≈20 and ≈90, respectively. For the first time, the impact of the diarylethene isomerization on hole and electron transport has been decoupled and directly investigated, via the design, fabrication, and characterization of single-carrier switchable devices based on the same blends. Not only do these results confirm the photoresponsive trapping activity of the diarylethenes on both charge carriers, but they also demonstrate its asymmetry, with a predominant effect on electron transport that is over 3.4 times larger as compared to hole transport.

1. Introduction

Organic thin film technologies have been widely developed for the last 30 years, and have now deeply penetrated the market, with an increasing impact expected for the upcoming decade.[1–3] Among them, organic light-emitting diodes (OLEDs) rapidly evolved from early prototypes[4] to a disrupting technology on the current display market.[5,6] Nevertheless, the scientific community continues to develop new classes of chromophores,[7–14] functional materials, and device architectures to further improve OLEDs performance or extend their application potential, as in visible light communications (VLCs).[15,16] Beside these efforts, there is emerging interest in stimuli-responsive organic devices, which can be controlled remotely by an external trigger, such as light.[17]

In organic thin film devices, light-responsivity can be introduced in the functional layers by embedding a photochromic compound, whose isomers are able to induce a distinct macroscopic effect on the optoelectronic properties of the device. A reversible modulation of such properties can be achieved by irradiating the device with photons of energy sufficient to trigger the reversible dopant photoisomerization process. The most prominent classes of photochromic compounds which have been used successfully in photo-switchable technologies are azobenzenes[18–22] and diarylethenes (DAEs).[20,21] In particular, DAEs show a number of properties which are highly desirable for the design and fabrication of a variety of responsive systems: i) vastly different optical, electrical, and energetic properties between the two, thermally stable, isomers; ii) highly reversible and fatigue

G. F. Cotella, G. Carnicella, A. Minotto, F. Cacialli
Department of Physics and Astronomy (CMMP Group) and London Centre for Nanotechnology
University College London
London WC1E 6BT, UK
E-mail: f.cacialli@ucl.ac.uk

The ORCID identification number(s) for the author(s) of this article can be found under https://doi.org/10.1002/adom.202101116.

DOI: 10.1002/adom.202101116

A. Bonasera, S. Hecht
Department of Chemistry & IRIS Adlershof
Humboldt-Universität zu Berlin
Brook-Taylor-Str. 2, 12489 Berlin, Germany

A. Bonasera
Department of Physics and Chemistry–Emilio Segrè
University of Palermo, and INSTM–Palermo Research Unit
viale delle Scienze, bdg. 17, Palermo 90128, Italy
E-mail: aurelio.bonasera@unipa.it

S. Hecht
DWI–Leibniz Institute for Interactive Materials
Forckenbeckstr. 50, 52074 Aachen, Germany
E-mail: hecht@dwi.rwth-aachen.de

S. Hecht
Institute of Technical and Macromolecular Chemistry
RWTH Aachen University
Worringer Weg 2, 52074 Aachen, Germany

resistant photochemical reactions, and iii) an extremely versatile chemical structure that allows fine tuning of the optical and electronic properties.[23–25] Thanks to the latter, DAEs are widely utilized as photo-responsive elements in a range of different applications such as photoactuation,[26–29] supramolecular assemblies,[30–33] biological binders,[34–37] and colorimetric probes.[38,39]

When DAEs are embedded in electronic or optoelectronic devices, the induced light-responsive behavior relies on the drastic variation of the dopants effective conjugation length induced by the isomerization, which in turn leads to a significant shift of the energy of their frontier molecular orbitals. Such a variation, when judiciously engineered, offers the potential for the reversible optical control of energy barriers and trap states for the charge carriers flowing through the device. Examples of light-responsive not-emissive devices involving DAEs derivatives are memory devices[40] and transistors.[41–43]

The very first attempts to incorporate DAEs into an OLED are relatively recent considered that both the DAEs chemistry and the OLED technology have been known for more than 30 years.[4,23,24] In 2008, Zhang et al. published the first work taking advantage of DAEs photochromism to modulate OLEDs performance.[44] In that work, a thermally evaporated device incorporated a layer of a pristine DAE derivative to realize a switchable energy barrier for positive carriers. Electroluminescence (with a turn-on voltage V_{ON} of 12 V) was visible only after UV irradiation due to the favorable band alignment of the closed DAEs with the other functional materials.

One year later, a similar design strategy was followed by the Meerholz group to fabricate solution-processed switchable blue-emitting OLEDs leveraging newly designed cross-linkable DAE-based hole-injection materials.[45] Notably, a combination of hole injection layers enabled a maximum device current density ON–OFF ratio (defined as the ratio between the current density in the ON and OFF states) of ≈ 300. Their multilayer approach was necessary since blending the DAEs derivative directly into the emitting polymer led to an irreversible reduction of the device electroluminescence efficiency and loss of photo-responsivity.

In 2015, Qian and coworkers presented a work on a light-responsive OLED based on DAEs blended in a multicomponent emissive layer (EML).[46] Remarkably, they achieved the reversible optical patterning of the device emissive area on the microscale. Here, the complexity of the EML did not allow them to identify a single origin of the device light-responsivity, which eventually was ascribed to a combination of hole trapping and energy transfer processes. More recent studies were focused on stimuli responsive light-emitting transistors,[43] or moved in the direction of limiting the amount of the photoswitchable motif, by means of preparing self-assembled monolayers[47] to modulate OLEDs performance via functionalized electrodes.[48]

With the aim to elucidate the impact of DAEs isomerization on the transport of the different charge carriers, here we report the design, fabrication, and characterization of optically switchable organic light-emitting diodes (OSOLEDs) based on an active bi-component layer, consisting of the highly investigated emissive polymer poly(9,9′-dioctylfluorene-*alt*-benzothiadiazole) (F8BT) and a specific photochromic DAE that locally generates trap states for both charge carriers types. For the first time, we investigated the effect of the DAEs isomerization on the transport of both electrons and holes via the characterization of specifically designed optically switchable single-carrier devices.

2. Results and Discussion

We selected the materials for the EML blend by considering the following aspects. First of all, we decided to use F8BT as the host material, as this is known to be a well performing fluorescent polymer that has been largely studied and used for its electron-transport properties.[49–51] The light-responsivity was achieved by selecting DAEs as photochromic switches, which are known to exhibit high fatigue resistance to the switching cycles and the ability to reach up to 96% of closed-isomer at the photostationary state (PSS).[25,52] Building on our previous studies on the modulation of frontier molecular orbital energy levels in DAEs,[53] we identified a specific DAE derivative carrying a fluorinated bridge and trifluoromethylated arms (hereafter simply named DAE), which exhibits the desired energetics to be matched with F8BT. The molecular structures and optical characterization of these compounds are shown in **Figure 1**a. Indeed, the highest occupied molecular orbital (HOMO) and lowest unoccupied molecular orbital (LUMO) levels of the DAE closed isomer (c-DAE, photogenerated by UV irradiation) give rise to a type I heterojunction with the fluorescent matrix, as shown in Figure 1b. In this situation, the transport of both holes and electrons within the organic blend is hindered due to the photogeneration of intragap trap states at energies ≈200–300 meV from the host bandgap edges.[49,53] Conversely, the device irradiation with visible light triggers the reverse photochemical reaction switching the DAE back to its open form (o-DAE). In this case, both HOMO and LUMO levels of the dopant lay outside the F8BT bandgap, thus the charge transport in the matrix is restored.

To verify the retention of the photochromic activity of the dopant in the solid state, we investigated the absorption of a blend combining an optically inert polymer, that is, polystyrene (PS), and DAE (at 20 wt% concentration). Indeed, the negligible absorption of the PS in the visible range, facilitates the detection of the spectral variations due to the dopant isomerization. Such a blend was spun on amorphous silica and characterized via UV/vis absorption spectroscopy. Figure 1c,d shows the blend absorption spectra under UV and visible irradiation. We can observe how the absorption band in the visible range, a fingerprint of the DAE closed isomer, gradually grows under UV irradiation while it vanishes under visible light in the subsequent irradiation step. The study of the reaction reversibility and fatigue resistance in the solid state was carried out over four successive light irradiations, each of them long enough to switch the dopant in the PSS. Each spectrum collected was subtracted from the one recorded after the previous irradiation step and thus in the resulting difference spectra the unchanged matrix contribution can be eliminated (please see details in Figure S1a, Supporting Information). The symmetric curves (with respect to the x axis) obtained by plotting the resulting data, (see Figure S1b, Supporting Information) confirm that the high reversibility of the dopant photochromic reaction is retained also in the solid state.

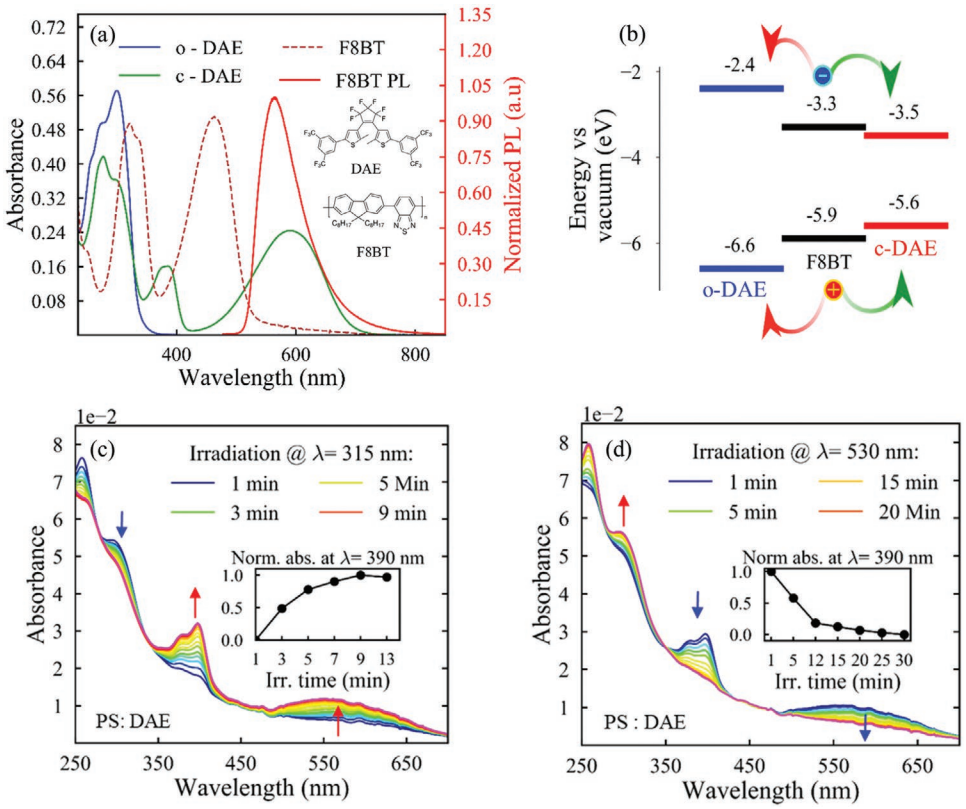

Figure 1. EML design and optical photoswitching: a) Absorption and normalized PL spectra of F8BT (host, thin film on amorphous silica) and photochromic guest (DAE, 5×10^{-5} M solution in acetonitrile), in the inset their molecular structures; b) HOMO–LUMO levels alignment after UV, $\lambda_{irr} = 315$ nm (red line) and VIS, $\lambda_{irr} = 528$ nm (blue line) irradiation. c) DAE optical switching in the solid state (PS:DAE 20 wt%) after UV and d) after VIS irradiation. c,d) Inset: the normalized absorption measured at 390 nm.

We studied the impact of the dopant photochromic activity also on the F8BT fluorescence. As shown in Figure S2a, Supporting Information, the F8BT:DAE 20 wt% blend emission drops systematically after UV irradiation (≈25%), while it fully recovers after visible irradiation. Such photoluminescence (PL) variation, which further confirms the DAEs' switchability in our blend, can be ascribed mainly to the host–guest spectral overlap that favors Förster resonant energy transfer (FRET) from the host to the essentially non-fluorescent guest,[39,54] as previously reported,[55,56] as well as to some minor degree of self-absorption. Exciton dissociation via transfer of one carrier species only to the DAE cannot be ruled out (also considering that the PL is obtained by exciting the host in the high-energy region of its Gaussianly distributed density of states), but we consider it is less favorable than energy transfer, given the type I nature of this heterojunction, and the frontier level mismatch that is expected to be somewhat smaller than the exciton binding energy ($E_B \approx 0.5$ eV). In contrast, the neat polymer (see Figure S2b, Supporting Information) does not show fluorescence modulation under light irradiation. Furthermore, as shown in Figure S3, Supporting Information, atomic force microscopy (AFM) carried out on thin films of neat F8BT and on the F8BT:DAE 10 wt% blend (the maximum doping used in our devices) did not show significant roughness variations connected to the presence of the dopant and its potential phase segregation.

Given the positive outcome of the preliminary investigations carried out on the photo-responsive blend, we fabricated solution-processed OSOLEDs based on F8BT:DAE blends with increasing concentrations of DAEs (1, 5, and 10 wt%), having the architecture ITO (150 nm)/PEDOT:PSS (40 nm)/F8BT:DAE (90 nm)/Ca (30 nm)/Al (150 nm), as illustrated in **Figure 2**a. The optoelectronic characterization, after UV and visible irradiation, of the least and most doped devices are reported in Figure 2b,c,e,f, respectively (see Figure S4, Supporting Information, for full data). Remarkably, the clear device light-responsivity is already visible with 1 wt% dopant concentration. As expected, the UV irradiation converts the DAEs to their closed form and they act as trap sites for the charge carriers, thus hindering transport through the blend and consequently increasing the device threshold voltage (V_{ON}), in line with previous reports.[44–46] Notably, the device performance, including its initial $V_{ON,}$ is almost fully recovered after the exposure to visible light that switches the DAEs back to the open form, thereby reducing the density of charge trap sites in our blends. Accordingly, the larger the dopant loading the larger is the induced reversible V_{ON} shift (calculated as the difference between the V_{ON} after UV irradiation and the V_{ON} after visible irradiation) as reported in the boxplot, in Figure 2d. This shows the statistics, for each blend, over successive irradiation steps, confirming the large device photo-tunability of our blends. In particular, the average V_{ON} shift is 2.1 ± 0.2 V for the least doped blend, and it

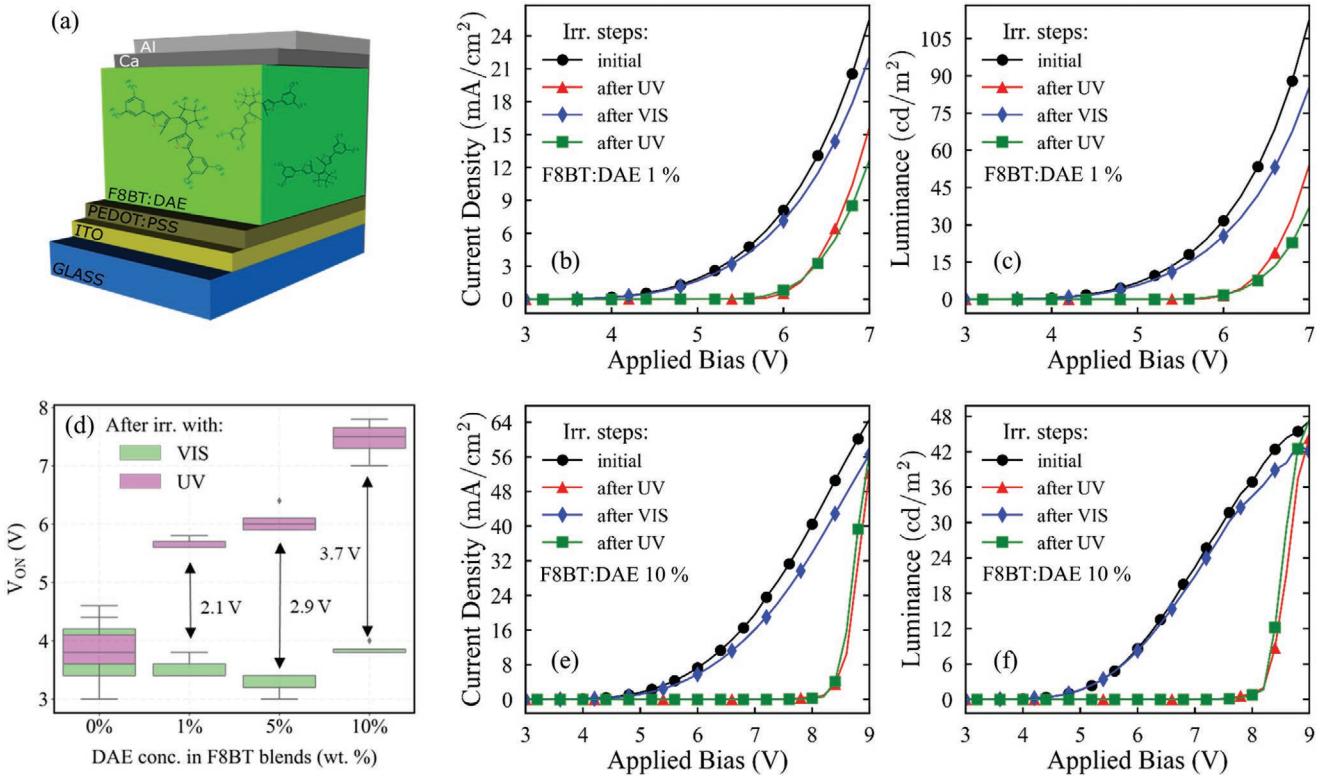

Figure 2. a) OSOLED device architecture. b,c) Reversible optical control of the current and luminance versus voltage behavior for OSOLEDs with a DAE loading of 1 wt% under irradiation with UV, $\lambda_{irr} = 315$ nm, and VIS, $\lambda_{irr} = 528$ nm light. d) Statistics over eight irradiation steps of the V_{ON} variation under UV, $\lambda_{irr} = 315$ nm, and VIS, $\lambda_{irr} = 528$ nm light for different DAE concentrations. e,f) Current and luminance versus voltage behavior for OSOLEDs with a DAE loading of 10 wt%. In plots b,c,e,f, the legend labels, from top to bottom, follow the chronological order of the irradiation steps. Markers on selected datapoints are guides to the eye.

doubles to 3.7 ± 0.3 V for devices incorporating the blend with 10 wt% DAE loading. This behavior is due to the increasing concentration of switchable trap sites within the blends. Interestingly, after UV irradiation, for biases larger than V_{ON}, the device current density and luminance values rise steeply to match the values measured after the visible irradiation. This observation can be explained by considering that once the photogenerated traps are filled, the electrons charge transport is expected to rapidly transit from the trap-limited regime to the space charge limited one (SCLC), therefore resulting in a sharp current density increment.[49,57–59] Furthermore, our devices display good fatigue resistance, as demonstrated by the retained device performance over multiple irradiation cycles (Figure S5, Supporting Information). Interestingly, the initially better performance of the OLED based on pure F8BT (Figure S4a,b, Supporting Information), drops to values comparable with or lower than those recorded for the other (switchable) devices, and does not show photo-modulation during the following irradiation steps. It is worth noticing that the used irradiation times are more suitable for smart signage applications than for VLCs. Nevertheless, we believe that a shortening of the irradiation time is still achievable by using a more intense light source[46,60] and by fabricating devices with thinner layer stacks in order to minimize the radiation necessary for DAE isomerization. Furthermore, DAE derivatives able to undergo faster isomerization reactions could be designed and employed.

The presence of the photochromic dopant in the EML does not have a strongly negative impact on the overall device performance for loadings up to 5 wt%. Indeed, the maximum external quantum efficiency (EQE), measured on devices after visible irradiation, was similar (0.17 ± 0.04%) across the different blends, with the exception of the most concentrated one (10 wt%) which showed a markedly lower EQE of ≈0.05% (Figure S7, Supporting Information). The best performing devices (DAE loading 5 wt%) showed maximum ON/OFF ratios of ≈20 and ≈90 for current density and luminance, respectively, and a maximum luminance of 151 cd m^{-2} (Figure S4c,d, Supporting Information). It is worth noticing that our devices were not optimized to achieve high performance, instead, a simpler device architecture was intentionally chosen to limit the contribution from unnecessary functional layers, such as hole- and electron-injection/transport layers. Additionally, the more demanding procedure for the full characterization of the switchable devices (compared to the non-switchable ones) might have had a detrimental impact on the long-term device performance. We expect that adding charge transport and injection layers to the device stack while maintaining the DAE concentration at 5 wt% (or lower) should improve the overall performance of our OSOLEDs. As expected, the F8BT electroluminescent (EL) spectrum is not altered by the presence of DAEs in the blend, as shown in Figure S6, Supporting Information. Although there is a non-negligible spectral overlap between the host (F8BT)

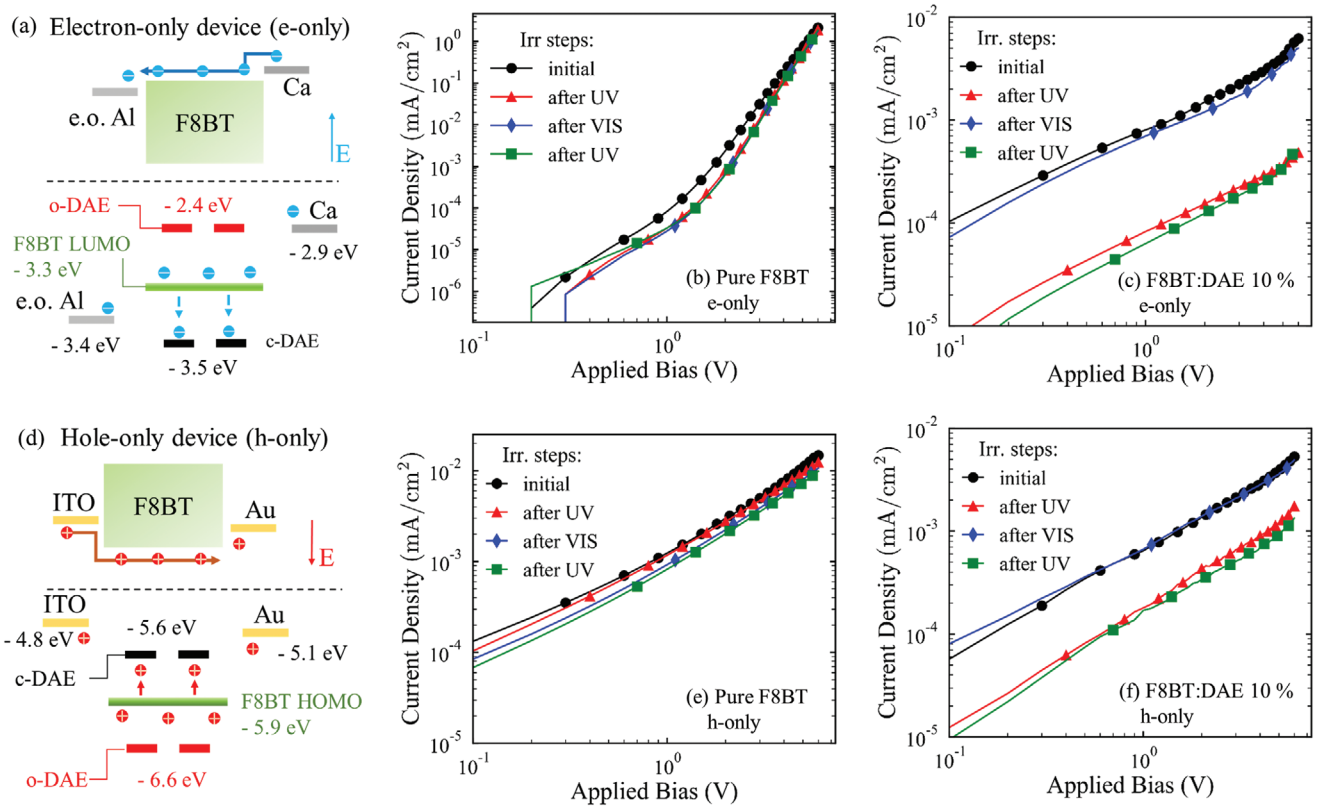

Figure 3. Optically switchable single carrier devices. a) Energetics in the electron-only device: top, F8BT LUMO-contacts WF alignment; bottom, schematic representation of the optically generated trap states for electrons. e.o. Al stands for "environmentally oxidized Al", o-DAE for "open DAE", and c-DAE for "closed DAE". d) Energetics in the hole-only device: top, F8BT HOMO-contacts WF alignment; bottom, schematic representation of optically generated trap states for holes. b,e) Device characteristics after light irradiation (UV: $\lambda_{irr} = 315$ nm, VIS: $\lambda_{irr} = 528$ nm) for the neat F8BT in electron- and hole-only device configurations, respectively. c,f) Device characteristics after light irradiation (UV: $\lambda_{irr} = 315$ nm, VIS: $\lambda_{irr} = 528$ nm) for the F8BT:DAE 10 wt% electron- and hole-only device configurations, respectively. In plots b,c,e,f, the legend labels, from top to bottom, follow the chronological order of the irradiation steps. Markers on selected datapoints are guides to the eye.

emission and the guest absorption spectra, the combined effect of a small concentration of the guest and of the well-established small quantum yield for the close-to-open isomerization (confirmed by the long-time needed for the isomerization processes, for example, as in the experiments reported in Figure 1) means that significant back-switching of the DAEs during the device characterization process is expected to be negligible, and we did not notice in fact any evidence to suggest the contrary. This is also in line with independent previous literature.[44]

To shed further light on the underlying phenomena regulating our device light-responsivity and eventually evaluate our EML design strategy, we fabricated switchable single-carrier devices to investigate the impact of DAE isomerization on the charge carrier transport. Additionally, the non-emissive nature of such devices, which clearly confirms their unipolar nature, allows us to exclude other potential influences on the device behavior such as FRET and self-absorption phenomena.[56] Such devices were based on the blend with 10 wt% loading of DAE as it gave the largest light-induced V_{ON} variation for ambipolar devices. Electron-only (e-only) devices had a semi-transparent layer of environmentally oxidized Al (eo-Al) as bottom electrode, as oxygen lowers the Al work function (WF) down to ≈3.4–3.7 eV,[61] and thus the architecture eo-Al (15 nm)/EML (90 nm)/Ca (30 nm)/Al (150 nm). Given the similar low WF of the electrodes, only electrons are favorably injected in the device and thus subjected to the optically switchable trapping process, as shown in **Figure 3**a. Differently, in hole-only (h-only) devices, to avoid the injection of electrons, the standard Ca cathode was replaced with Au (with a WF of ≈4.8–5.1 eV),[62] thus yielding the final architecture ITO (150 nm)/PEDOT:PSS (40 nm)/EML (90 nm)/Au (150 nm). Here the gold contact generates ≈1.5–1.8 eV energy barrier for the injection of electrons, which ensures that only holes will flow through the device and thus interact with the photochromic dopant (up to very large applied voltages, exceeding those used here), as illustrated in Figure 3d.

In Figure 3, we report the comparison between the current density–voltage (J–V) characteristics of single carrier devices based on F8BT, neat and blended with DAE. In the case of pristine F8BT (Figure 3b–e), no significant variation in the charge transport properties is detected following the light irradiation cycles, neither for electrons nor for holes. Interestingly, the maximum current density of electrons exceeds that of holes by two orders of magnitude. This behavior can be explained by considering that in our devices electrons are injected through an ohmic contact whereas holes through a rectifying one as shown in Figure 3a–d.[49,63] Indeed, the electronic characteristics (Figure 3b) show two typical different transport regimes: at

low voltages the transport is hindered by trap states, intrinsically present in disordered organic semiconductors, and then, once the carriers fill them, the current density sharply grows to reach the SCLC regime.[57] In contrast, in the h-only devices reported here, the charge transport is injection-limited due to residual hole-injection barriers with the selected electrodes.

Looking at the *J–V* plots (3c,f) of the heavily doped blend (10 wt%), and regardless of the light irradiation, we observe a reduction of the maximum current density measured with respect to the pure-F8BT devices. In particular, electron transport appears to be strongly affected by the presence of the photochromic dopants. Indeed, in the voltage range investigated, the device mainly remains in the trap-limited regime, thus the maximum current density drops by more than two orders of magnitude (from 7×10^{-1} to 3.8×10^{-3} mA cm^{-2}, evaluated at 5.0 V) compared to the undoped device. Conversely, we measured a lower drop, by ≈66%, in the case of the hole-only device.

Importantly, however, both doped single-carrier devices show a marked and fully reversible light-responsivity, as proof of simultaneous trap activity on each type of charge carriers. Upon irradiation (see Figure 3c,f) of e-only devices we measured a current density variation larger than one order of magnitude (from 3.8×10^{-3} to 3.1×10^{-4} mA cm^{-2}, evaluated at 5.0 V). Differently, in the case of hole-only devices, the current density is reversibly modulated by a 3.6 factor (from 4×10^{-3} to 1.1×10^{-3} mA cm^{-2}, evaluated at 5.0 V). The trapping of electrons induced by the photochromic dopant is thus more than 3.4 times larger than what measured for holes.

3. Conclusion

We successfully designed, fabricated and characterized solution-processed OSOLEDs based on F8BT and DAE and having a simple device architecture based on blending of the two components. We first assessed the retained DAEs photochromic activity in the solid state via UV and PL spectroscopy measurement. Then, we demonstrated the ability of our devices to be remotely controlled via optical stimuli achieving a maximum reversible device threshold voltage shift of 4 V. Our best performing device showed a maximum ON/OFF ratio of ≈20 and ≈90, for current density and luminance, respectively. Importantly, we designed our EML for the generation of optically switchable trap sites for both holes and electrons and, for the first time, we directly assessed the trapping process via the characterization of switchable single-carrier devices. Our data confirm the marked charge trapping activity on both carriers, and, crucially, also demonstrate that electrons are predominantly affected. Our optically switchable electron-only devices gave, under the same irradiation conditions and trap-state energies, a reversible current/luminance modulation over 3.4 times larger than that observed for the hole-only devices.

This work contributes to the deeper understanding of the design strategy and driving mechanisms of light-responsive devices. For the first time, via direct investigation of the trapping mechanism in both ambipolar and unipolar devices based on the same blends, the trapping process acting on each charge carrier type has been decoupled and evaluated. Our results pave the way for further optimization of device performance to aid potential commercialization of multi-functional OSOLEDs for smart applications, such as displays, signage, VLC systems, and photosensors.

4. Experimental Section

Materials and Substrates Treatments: Poly(9,9′-dioctylfluorene-*alt*-benzothiadiazole) (F8BT, 1:1 copolymer, $M_w \approx 256\,000$ g mol^{-1}) was purchased from Ossila and used as received; PS ($M_w \approx 350\,000$ g mol^{-1}), poly(3,4-ethylenedioxythiophene) polystyrene sulfonate (PEDOT:PSS-Al 4083), solvents and chemicals used for the DAE dopant preparation were purchased from Sigma-Aldrich (subsidiary of Merck KGaA, St. Louis, US-MO) and used as received. Synthesis of the final target molecule was carried out according to previously reported procedures.[25] The characterization of the final product confirms the previously reported spectral data and mass analyses. The electrochemical characterization carried out to determine the position of the DAE frontier orbitals was reported previously,[53] and the experimental setup has been described in detail in the literature.[53,64] Fused silica and ITO-coated glass substrates (20 Ω sq^{-1}) were purchased from Ossila Ltd (Sheffield, UK); the substrates were cleaned via ultrasonication in different solvents (5 min each) having decreasing polarity (deionized water, acetone, and 2-propanol). After drying in a flow of nitrogen, the substrates underwent a 10 min long oxygen plasma treatment (PDC-002 model, Harrick Plasma Inc., Ithaca, US-NY), at an oxygen pressure of 1.1×10^{-1} mbar.[65]

Thin Film Deposition, Optical, and Morphological Characterization: In a nitrogen-filled Mbraun glovebox, F8BT and DAE were dissolved in anhydrous toluene and chloroform (10 mg mL^{-1}), respectively, left stirring overnight, filtered via a PTFE filter (pores of 0.2 µm) and then used to prepare blends F8BT:DAE having concentrations of 1, 5, 10, and 20 wt%. After stirring for further 3 h, F8BT and the blends solutions were spin-coated (1200 rpm, thickness of ≈100 nm) on fused silica substrates for optical and morphological investigations. Following the same procedure, PS was dissolved in chlorobenzene to a concentration of 50 mg mL^{-1} and used to prepare the PS:DAE blend with 20 wt% concentration. Film thicknesses were measured using a Bruker Dektak stylus profilometer (Bruker, Billerica, US-MA). Surface morphology investigation of the blends under study has been performed in air via AFM (Bruker Dimension Icon—PeakForce tapping mode) on an area of 1 µm^2. The absorption spectra after UV (≈9 min) and visible (≈15 min) irradiation were collected using an Agilent 8453 spectrophotometer (Agilent Technologies Inc., Santa Clara, US-CA). LEDs emitting in the visible (528 nm, 7 mW) and UV (315 nm, 0.6 mW) were fixed on the equipment and connected to a microcontroller to allow the in situ sample irradiation. Using the same irradiation conditions as the UV/vis absorption measurement, the PL spectra of pure F8BT and F8BT:DAE 20 wt% blend, in the solid state, were measured in air, at room temperature. The photoexcitation at 450 nm was provided by a Xe lamp coupled with a Bentham monochromator, the spectra were collected with an Oxford Instruments ANDOR-Shamrock 163 spectrometer coupled with an ANDOR-Newton charge-coupled device (CCD) unit (Oxford Instruments, Abingdon-on-Thames, UK).

Device Fabrication and Characterization: ITO coated glass substrates were cleaned and treated via O_2 plasma as described above. This allows thorough cleaning of the surface and an overall increase of the ITO WF.[66,67] The hole injection layer (PEDOT:PSS from Sigma Aldrich) was filtered, through a 0.2 µm porous filter, and spin-coated at 4000 rpm to a thickness of ≈40 nm. The sample was then baked at 170 °C for 10 min in N_2 atmosphere. The emitting layers were spin-coated at 1200 rpm to a thickness of ≈100 nm. The layers thicknesses were determined via profilometric measurements. A 30 nm thick Ca electrode and a 150 nm thick capping layer of Al were thermally evaporated in high vacuum (10^{-6} mbar). Devices were encapsulated in the glovebox using glass coverslips and UV-curable epoxy resin. Single carrier devices: in case of hole-only devices the Ca/Al top electrode was substituted with a thermally evaporated, 150 nm thick, Au electrode. For electron-only

device a semitransparent, 15 nm thick, Al layer was deposited as bottom electrode. Substrates were exposed to air overnight and then annealed in the glovebox at 150 °C for 10 min to remove water residues. EML and top-contact were deposited as described for ambipolar devices.

To assess device switchability, commercial LEDs emitting in the visible (λ_{irr} = 528 nm, 7 mW) and UV (λ_{irr} = 315 nm, 0.6 mW) were used to irradiate the devices for 9 and 15 min respectively. For each device, a number of preliminary voltage scans and short irradiation steps were carried out to verify the presence of light responsivity. The devices under tests (OSOLEDs and controls) were irradiated with visible light (9 min) before starting the switching cycles reported. After each irradiation, such devices were characterized by using a Keithley 2400 source meter (Tektronix, Inc., Beaverton, US-OR) for both the current measurement and the voltage supply. The optical output of the PLEDs was measured with a calibrated silicon photodiode connected to a Keithley 2000 multimeter. The device V_{ON} is extracted as the voltage where the luminance is ten times the noise level. The EL spectrum was collected with an ANDOR-Shamrock spectrograph coupled with an ANDOR-Newton CCD unit.

Supporting Information

Supporting Information is available from the Wiley Online Library or from the author.

Acknowledgements

The authors thank Jana Hildebrandt for synthetic support. The authors acknowledge funding from the European Commission through the Marie Sklodowska-Curie ITN project iSwitch (GA-642196), the Marie Skłodowska-Curie ITN project SYNCHRONICS (GA-643238), ERC project LIGHT4FUNCTION (GA-308117), from the DFG (project 182087777 - SFB 951) and EPSRC (grant EP/P006280/1, MARVEL, and EP/P007767/1 CAM-IES). F.C. acknowledges receipt of a Royal Society Wolfson Research Merit Award.

Conflict of Interest

The authors declare no conflict of interest.

Data Availability Statement

Research data are not shared.

Keywords

blends, diarylethenes, F8BT, photochromism, stimuli-responsive OLEDs

Received: June 2, 2021
Revised: September 23, 2021
Published online:

[1] J. S. Lewis, M. S. Weaver, *IEEE J. Sel. Top. Quantum Electron.* **2004**, *10*, 45.
[2] B. Kippelen, J.-L. Brédas, *Energy Environ. Sci.* **2009**, *2*, 251.
[3] G. Gelinck, P. Heremans, K. Nomoto, T. D. Anthopoulos, *Adv. Mater.* **2010**, *22*, 3778.
[4] C. W. Tang, S. A. VanSlyke, *Appl. Phys. Lett.* **1987**, *51*, 913.
[5] L. S. Hung, C. H. Chen, *Mater. Sci. Eng., R* **2002**, *39*, 143.
[6] H. Sasabe, J. Kido, *Eur. J. Org. Chem.* **2013**, *2013*, 7653.
[7] W. Y. Hung, P. Y. Chiang, S. W. Lin, W. C. Tang, Y. T. Chen, S. H. Liu, P. T. Chou, Y. T. Hung, K. T. Wong, *ACS Appl. Mater. Interfaces* **2016**, *8*, 4811.
[8] R. Kabe, N. Notsuka, K. Yoshida, C. Adachi, *Adv. Mater.* **2016**, *28*, 655.
[9] S. Y. Lee, C. Adachi, T. Yasuda, *Adv. Mater.* **2016**, *28*, 4626.
[10] Y. Seino, S. Inomata, H. Sasabe, Y. J. Pu, J. Kido, *Adv. Mater.* **2016**, *28*, 2638.
[11] J. Yang, J. Huang, Q. Li, Z. Li, *J. Mater. Chem. C* **2016**, *4*, 2663.
[12] J. Huang, H. Nie, J. Zeng, Z. Zhuang, S. Gan, Y. Cai, J. Guo, S. J. Su, Z. Zhao, B. Z. Tang, *Angew. Chem.* **2017**, *129*, 13151; *Angew. Chem., Int. Ed.* **2017**, *56*, 12971.
[13] M. Y. Wong, E. Zysman-Colman, *Adv. Mater.* **2017**, *29*, 1605444.
[14] Z. Yang, Z. Mao, Z. Xie, Y. Zhang, S. Liu, J. Zhao, J. Xu, Z. Chi, M. P. Aldred, *Chem. Soc. Rev.* **2017**, *46*, 915.
[15] P. A. Haigh, F. Bausi, Z. Ghassemlooy, I. Papakonstantinou, H. L. Minh, C. Fléchon, F. Cacialli, *Opt. Express* **2014**, *22*, 2830.
[16] A. Minotto, P. A. Haigh, Ł. G. Łukasiewicz, E. Lunedei, D. T. Gryko, I. Darwazeh, F. Cacialli, *Light: Sci. Appl.* **2020**, *9*, 2047.
[17] A. Goulet-Hanssens, F. Eisenreich, S. Hecht, *Adv. Mater.* **2020**, *32*, 1905966.
[18] J. Kim, H. J. Park, S. I. Na, Y. Y. Noh, D. Y. Kim, *Jpn. J. Appl. Phys.* **2014**, *53*, 4.
[19] K. D. Renuka, C. Lalitha Lekshmi, K. Joseph, S. Mahesh, *ACS Appl. Mater. Interfaces* **2017**, *9*, 1167.
[20] M. Bremer, C. Kallweit, A. F. K. Iwers, M. Gerken, *IEEE Photonics Technol. Lett.* **2018**, *30*, 673.
[21] J. C. Lai, W. F. Cheng, C. K. Liu, K. T. Cheng, *Dyes Pigm.* **2019**, *163*, 641.
[22] N. Crivillers, A. Liscio, F. Di Stasio, C. Van Dyck, S. Osella, D. Cornil, S. Mian, G. M. Lazzerini, O. Fenwick, E. Orgiu, F. Reinders, S. Braun, M. Fahlman, M. Mayor, J. Cornil, V. Palermo, F. Cacialli, P. Samorì, *Phys. Chem. Chem. Phys.* **2011**, *13*, 14302.
[23] M. Irie, *Chem. Rev.* **2000**, *100*, 1685.
[24] M. Irie, T. Fukaminato, K. Matsuda, S. Kobatake, *Chem. Rev.* **2014**, *114*, 12174.
[25] M. Herder, B. M. Schmidt, L. Grubert, M. Pätzel, J. Schwarz, S. Hecht, *J. Am. Chem. Soc.* **2015**, *137*, 2738.
[26] S. Kobatake, S. Takami, H. Muto, T. Ishikawa, M. Irie, *Nature* **2007**, *446*, 778.
[27] F. Terao, M. Morimoto, M. Irie, *Angew. Chem.* **2012**, *124*, 925; *Angew. Chem., Int. Ed.* **2012**, *51*, 901.
[28] D. Kitagawa, H. Nishi, S. Kobatake, *Angew. Chem.* **2013**, *125*, 9490; *Angew. Chem., Int. Ed.* **2013**, *52*, 9320.
[29] S. Ohshima, M. Morimoto, M. Irie, *Chem. Sci.* **2015**, *6*, 5746.
[30] T. Hirose, M. Irie, K. Matsuda, *Adv. Mater.* **2008**, *20*, 2137.
[31] J. Kärnbratt, M. Hammarson, S. Li, H. L. Anderson, B. Albinsson, J. Andréasson, *Angew. Chem.* **2010**, *122*, 1898; *Angew. Chem., Int. Ed.* **2010**, *49*, 1854.
[32] S. Yagai, K. Iwai, M. Yamauchi, T. Karatsu, A. Kitamura, S. Uemura, M. Morimoto, H. Wang, F. Würthner, *Angew. Chem.* **2014**, *126*, 2640; *Angew. Chem., Int. Ed.* **2014**, *53*, 2602.
[33] M. Han, Y. Luo, B. Damaschke, L. Gómez, X. Ribas, A. Jose, P. Peretzki, M. Seibt, G. H. Clever, *Angew. Chem.* **2016**, *128*, 456; *Angew. Chem., Int. Ed.* **2016**, *55*, 445.
[34] D. Vomasta, C. Högner, N. R. Branda, B. König, *Angew. Chem.* **2008**, *120*, 7756; *Angew. Chem., Int. Ed.* **2008**, *47*, 7644.
[35] C. Falenczyk, M. Schiedel, B. Karaman, T. Rumpf, N. Kuzmanovic, M. Grøtli, W. Sippl, M. Jung, B. König, *Chem. Sci.* **2014**, *5*, 4794.
[36] B. Reisinger, N. Kuzmanovic, P. Löffler, R. Merkl, B. König, R. Sterner, *Angew. Chem.* **2014**, *126*, 606; *Angew. Chem., Int. Ed.* **2014**, *53*, 595.
[37] O. Babii, S. Afonin, L. V. Garmanchuk, V. V. Nikulina, T. V. Nikolaienko, O. V. Storozhuk, D. V. Shelest, O. I. Dasyukevich,

L. I. Ostapchenko, V. Iurchenko, S. Zozulya, A. S. Ulrich, I. V. Komarov, *Angew. Chem.* **2016**, *128*, 5583; *Angew. Chem., Int. Ed.* **2016**, *55*, 5493.
[38] V. Valderrey, A. Bonasera, S. Fredrich, S. Hecht, *Angew. Chem.* **2017**, *129*, 1941; *Angew. Chem., Int. Ed.* **2017**, *56*, 1914.
[39] S. Fredrich, A. Bonasera, V. Valderrey, S. Hecht, *J. Am. Chem. Soc.* **2018**, *140*, 6432.
[40] R. C. Shallcross, P. O. Körner, E. Maibach, A. Köhnen, K. Meerholz, *Adv. Mater.* **2013**, *25*, 4807.
[41] E. Orgiu, N. Crivillers, M. Herder, L. Grubert, M. Pätzel, J. Frisch, E. Pavlica, D. T. Duong, G. Bratina, A. Salleo, N. Koch, S. Hecht, P. Samorì, *Nat. Chem.* **2012**, *4*, 675.
[42] K. Börjesson, M. Herder, L. Grubert, D. T. Duong, A. Salleo, S. Hecht, E. Orgiu, P. Samorì, *J. Mater. Chem. C* **2015**, *3*, 4156.
[43] L. Hou, X. Zhang, G. F. Cotella, G. Carnicella, M. Herder, B. M. Schmidt, M. Pätzel, S. Hecht, F. Cacialli, P. Samorì, *Nat. Nanotechnol.* **2019**, *14*, 347.
[44] Z. Zhang, X. Liu, Z. Li, Z. Chen, F. Zhao, F. Zhang, C. H. Tung, *Adv. Funct. Mater.* **2008**, *18*, 302.
[45] P. Zacharias, M. C. Gather, A. Köhnen, N. Rehmann, K. Meerholz, *Angew. Chem.* **2009**, *121*, 4098; *Angew. Chem., Int. Ed.* **2009**, *48*, 4038.
[46] Y. Qian, X. Xu, W. Li, J. Wang, B. Wei, Q. Wei, X. Yan, W. Hu, Y. Lu, L. Xie, X. Zhang, W. Huang, *Org. Electron.* **2015**, *26*, 476.
[47] Q. Wang, V. Diez-Cabanes, S. Dell'Elce, A. Liscio, B. Kobin, H. Li, J.-L. Brédas, S. Hecht, V. Palermo, E. J. W. List-Kratochvil, J. Cornil, N. Koch, G. Ligorio, *ACS Appl. Nano Mater.* **2019**, *2*, 1102.
[48] G. Ligorio, G. F. Cotella, A. Bonasera, N. Zorn Morales, G. Carnicella, B. Kobin, Q. Wang, N. Koch, S. Hecht, E. J. W. List-Kratochvil, F. Cacialli, *Nanoscale* **2020**, *12*, 5444.
[49] Y. Zhang, P. W. M. Blom, *Appl. Phys. Lett.* **2011**, *98*, 143504.
[50] A. Dey, A. Rao, D. Kabra, *Adv. Opt. Mater.* **2017**, *5*, 1600678.
[51] A. J. Campbell, D. D. C. Bradley, H. Antoniadis, *Appl. Phys. Lett.* **2001**, *79*, 2133.
[52] J. Frisch, M. Herder, P. Herrmann, G. Heimel, S. Hecht, N. Koch, *Appl. Phys. A* **2013**, *113*, 1.
[53] M. Herder, F. Eisenreich, A. Bonasera, A. Grafl, L. Grubert, M. Pätzel, J. Schwarz, S. Hecht, *Chem. - Eur. J.* **2017**, *23*, 3743.
[54] C. Yun, J. You, J. Kim, J. Huh, E. Kim, *J. Photochem. Photobiol., C* **2009**, *10*, 111.
[55] S. Perissinotto, M. Garbugli, D. Fazzi, C. Bertarelli, M. Carvelli, A. R. Srimath Kandada, Z. Yue, K. S. Wong, G. Lanzani, *ChemPhysChem* **2011**, *12*, 3619.
[56] R. Schmidt, M. Pärs, T. Weller, M. Thelakkat, J. Köhler, *Appl. Phys. Lett.* **2014**, *104*, 013304.
[57] P. W. M. Blom, M. J. M. De Jong, J. J. M. Vleggaar, *Appl. Phys. Lett.* **1996**, *68*, 3308.
[58] M. M. Mandoc, B. De Boer, G. Paasch, P. W. M. Blom, B. de Boer, G. Paasch, P. W. M. Blom, *Phys. Rev. B* **2007**, *75*, 12.
[59] R. Steyrleuthner, S. Bange, D. Neher, *J. Appl. Phys.* **2009**, *105*, 064509.
[60] T. Leydecker, M. Herder, E. Pavlica, G. Bratina, S. Hecht, E. Orgiu, P. Samorì, *Nat. Nanotechnol.* **2016**, *11*, 769.
[61] R. I. R. Blyth, S. A. Sardar, F. P. Netzer, M. G. Ramsey, *Appl. Phys. Lett.* **2000**, *77*, 1212.
[62] D. R. Lide, *CRC Handbook of Chemistry and Physics: A Ready-Reference Book of Chemical and Physical Data*, CRC Press, Boca Raton, FL **1995**.
[63] L. Wan, J. Wade, F. Salerno, O. Arteaga, B. Laidlaw, X. Wang, T. Penfold, M. J. Fuchter, A. J. Campbell, *ACS Nano* **2019**, *13*, 8099.
[64] J. W. Chung, S.-J. Yoon, S.-J. Lim, B.-K. An, S. Y. Park, *Angew. Chem.* **2009**, *121*, 7164; *Angew. Chem., Int. Ed.* **2009**, *48*, 7030.
[65] T. M. Brown, G. M. Lazzerini, L. J. Parrott, V. Bodrozic, L. Bürgi, F. Cacialli, *Org. Electron.* **2011**, *12*, 623.
[66] N. Johansson, F. Cacialli, K. Z. Xing, G. Beamson, D. T. Clark, R. H. Friend, W. R. Salaneck, *Synth. Met.* **1998**, *92*, 207.
[67] J. S. Kim, F. Cacialli, M. Granström, R. H. Friend, N. Johansson, W. R. Salaneck, R. Daik, W. J. Feast, *Synth. Met.* **1999**, *101*, 111.